

Entanglement and correlations in fast collective neutrino flavor oscillationsAlessandro Roggero^{1,2,3,*}, Ermal Rrapaj^{4,†} and Zewei Xiong^{5,‡}¹*InQubator for Quantum Simulation (IQUS), Department of Physics, University of Washington, Seattle, Washington 98195, USA*²*Dipartimento di Fisica, University of Trento, via Sommarive 14, I-38123 Povo, Trento, Italy*³*INFN-TIFPA Trento Institute of Fundamental Physics and Applications, 38123 Trento, Italy*⁴*Department of Physics, University of California, Berkeley, California 94720, USA*⁵*GSI Helmholtzzentrum für Schwerionenforschung, 64291 Darmstadt, Germany*

(Received 29 March 2022; accepted 2 August 2022; published 24 August 2022)

Collective neutrino oscillations play a crucial role in transporting lepton flavor in astrophysical settings like supernovae and neutron star binary merger remnants, which are characterized by large neutrino densities. In these settings, simulations in the mean-field approximation show that neutrino-neutrino interactions can overtake vacuum oscillations and give rise to fast collective flavor evolution on timescales $t \propto \mu^{-1}$, with μ proportional to the local neutrino density. In this work, we study the full out-of-equilibrium flavor dynamics in simple multiangle geometries displaying fast oscillations in the mean field linear stability analysis. Focusing on simple initial conditions, we analyze the production of pair correlations and entanglement in the complete many-body-dynamics as a function of the number N of neutrinos in the system, for up to thousands of neutrinos. Similarly to simpler geometries with only two neutrino beams, we identify three regimes: stable configurations with vanishing flavor oscillations, marginally unstable configurations with evolution occurring on long timescales $\tau \approx \mu^{-1}\sqrt{N}$, and unstable configurations showing flavor evolution on short timescales $\tau \approx \mu^{-1} \log(N)$. We present evidence that these fast collective modes are generated by the same dynamical phase transition which leads to the slow bipolar oscillations, establishing a connection between these two phenomena and explaining the difference in their timescales. We conclude by discussing a semiclassical approximation which reproduces the entanglement entropy at short to medium timescales and can be potentially useful in situations with more complicated geometries where classical simulation methods starts to become inefficient.

DOI: [10.1103/PhysRevD.106.043022](https://doi.org/10.1103/PhysRevD.106.043022)**I. INTRODUCTION**

Neutrinos are some of the most abundant particles found in nature, produced during the early universe [1–4], from stars like the sun during their lifetime [5], and in copious amounts during core collapse supernovae [6–11]. Neutrino flavor conversions, or oscillations, are genuine quantum mechanical phenomena for which a flavor eigenstate is converted to another during propagation due to it being an admixture of different mass eigenstates.

In core-collapse supernovae (CCSNe) and neutron star merger remnants, neutrinos are responsible for both reinvigorating a stalled shock-wave and controlling the conditions for nucleosynthesis in the ejected material [12–15]. In these environments neutrino flavor evolution is substantially modified by the presence of neutrino-neutrino scattering processes which can lead to self-sustained collective

flavor oscillations [16–24]. Since neutrinos in supernovae are emitted with fluxes and spectra that are strongly flavor dependent [13], the presence of collective flavor oscillations could then lead to important effects [25–38]. Neutrino-neutrino scattering, being between particles of the same type, is of a different nature than neutrino-matter scattering, and gives rise to forward scattering terms in the many-body Hamiltonian which contribute to oscillations [17,39]. These terms are dependent only on the angle between neutrinos and couple neutrinos of different energies making flavor evolution a rather intricate many-body problem. Thanks to the adoption of a mean-field approximation, a rich phenomenology of collective neutrino modes have been identified (see [40,41] for reviews). In particular two main classes of collective modes have been categorized as the slow and fast modes of flavor instability based on the triggering mechanism and the typical length scale of the flavor transition. Slow modes are due to the interference of the vacuum flavor mixing and neutrino-neutrino self-induced forward scattering. The respective conversion rate is $\sim \sqrt{\omega\mu}$, where $\omega = \Delta m^2/2E_\nu$ is the vacuum oscillation frequency for neutrinos

*a.roggero@unitn.it

†ermalrappaj@gmail.com

‡z.xiong@gsi.de

of energy E_ν with mass square difference Δm^2 , and $\mu = \sqrt{2}G_F\rho_\nu$ indicates the magnitude of self-induced effective potential with Fermi constant G_F and neutrino number density ρ_ν . Slow flavor evolution typically shows a bipolar behavior in terms of the flavor survival probability and usually results in drastic splitting of neutrino spectra [28,40–42]. Fast flavor conversions can occur even in the absence of vacuum mixing since it is enabled by nontrivial angular distributions and the consequent flavor evolution has a strong angular dependence. The associated flavor conversion rate is $\sim\mu$, much faster than the slow mode when the neutrino number density ρ_ν is high and $\mu \gg \omega$ as, for example, near the proto-neutron star of CCSNe or the hyper-massive star of merger remnants [43–50].

In this work we study collective oscillations of two active neutrino flavors, under only the influence of the Hamiltonian induced by neutrino-neutrino interactions. We assume a simplified scenario of electron neutrinos ν_e , and an additional flavor which can be considered as a superposition of tau and muon neutrinos denoted by ν_x , with no vacuum mixing (or high neutrino density) and only focus on the effects of neutrino forward scattering. To simplify the treatment, we consider a three beam setup as explained in Sec. II. We note in passing that antineutrinos would also be present in a realistic scenario. However, in our setting without vacuum mixing, antineutrinos play the same role as neutrinos of the other flavor ($\bar{\nu}_{e,x} \leftrightarrow \nu_{x,e}$). With N_f flavors and neglecting momentum-changing interactions, the many-body Hamiltonian can be formulated in terms of $SU(N_f)$ operators acting on the flavor state of neutrinos. This approach is particularly useful for studying many-body effects. In Sec. III we perform a linear stability analysis in the mean field approximation to determine which configurations are unstable under perturbations, and proceed to explain the many-body methods used in the work in Sec. IV. The results for the flavor evolution for the various setup and increasing particle number are summarized in Sec. V. In Sec. VI we focus on the dynamical creation of entanglement entropy and correlations from the initial mean field wave function. The findings are summarized and conclusions are drawn in Sec. VII.

II. THREE BEAM GEOMETRY AND HAMILTONIAN

As our focus here is on the many-body effects, we consider only the flavor evolution of neutrinos under $\nu - \nu$ forward scattering and ignore the vacuum term or scattering with matter. In studies of collective and fast neutrino flavor oscillations, this is a common choice as the flavor instability is assumed to originate from this part of the total Hamiltonian, with an initial “seed” from the other terms [44–47,51–54]. The presence of this perturbation is required to ensure flavor evolution within the mean-field approximation, while in a full many-body simulation the seed is effectively provided by quantum fluctuations. As shown

in detail in Ref. [55] for the simpler case of a two beam model, the size of the seed controls the rate of convergence of the full quantum many-body simulation to the mean-field prediction. Mapping out the detailed dependence of the many-body results on this additional parameter is left for future explorations as the models explored here are already relatively complicated and we aim at describing beyond mean-field effects only as was done in Refs. [56,57]. This work is the first attempt at uncovering the neutrino-neutrino correlations and quantum entanglement using the complete many-body treatment of this dynamics under the influence of multiangle effects. Accounting only for forward scattering, the Hamiltonian governing flavor evolution can thus be expressed in the following form [58]

$$H = \frac{\mu}{N} \sum_{i \neq j}^N (1 - c_{ij}) \mathbf{J}_i \cdot \mathbf{J}_j \quad (1)$$

with N the total particle number and $c_{ij} = \cos(\theta_{ij})$ the cosine of the angle between the momenta of neutrinos i and j . The interactions between neutrinos propagating in parallel directions therefore vanishes. The coupling constant $\mu = \sqrt{2}G_F\rho_\nu$ depends on both Fermi’s constant G_F and the local neutrino density ρ_ν . Here we work in the approximation where neutrinos have only two possible flavors and their state can be specified using a two component isospin degree of freedom. The single particle operators acting on these flavor states form an $SU(2)$ algebra and can be expressed using isospin operators

$$\mathbf{J}_i = \frac{1}{2} (\sigma_i^x, \sigma_i^y, \sigma_i^z), \quad (2)$$

with σ_i^k the k th Pauli matrix acting on the i th particle. To study the large particle number limit, we assume a constant neutrino density ρ_ν , and the system to be comprised of several neutrino beams. Each beam contains many neutrinos with momenta aligned to each other, a configuration made possible by assigning different energies to the neutrinos in the beam in order to satisfy their fermionic antisymmetry. We then define flavor isospin operators for beams as

$$\mathbf{J}_\alpha = \sum_{i \in \alpha} \mathbf{J}_i, \quad (3)$$

where the sum runs over the N_α particles belonging to the beam $\alpha \in \{A, B, C, \dots\}$. Here and in the rest of this work we will use greek letters to refer to beams and (lower-case) latin letters to refer to individual neutrinos. Since $[H, \mathbf{J}_\alpha^2] = 0$, the total flavor isospin of each beam is conserved and, for initial states that are eigenstates of \mathbf{J}_α^2 , we can express the nontrivial part of the Hamiltonian from Eq. (1) in terms of beam operators as follows

$$H = \frac{\mu}{N} \sum_{\alpha \neq \beta}^n (1 - c_{\alpha\beta}) \mathbf{J}_\alpha \cdot \mathbf{J}_\beta, \quad (4)$$

where n is the number of beams and have neglected irrelevant additive constant terms. This system has many symmetries

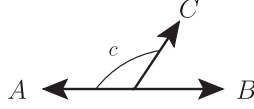


FIG. 1. Beams A and B are antiparallel, and beam C forms an angle θ_{AC} with beam A .

worth pointing out. In addition to the individual \mathbf{J}_α^2 being conserved, also the total angular momentum \mathbf{J}^2 and total \mathbf{J} commute with the Hamiltonian.

For simplicity, we will take $n = 3$ beams and assume an equal number of neutrinos in each beam with $N_\alpha = N/3$. We further consider the direction of propagation in these three beams to lie on a plane and that two of them are antiparallel. This simple angular configuration is shown in Fig. 1 and is parametrized by a single angle θ_{AC} .

The Hamiltonian then becomes (see Appendix A)

$$H_{ABC} = \frac{4\mu}{N} \mathbf{J}_A \cdot \mathbf{J}_B + \frac{2\mu}{N} (1-c) \mathbf{J}_A \cdot \mathbf{J}_C + \frac{2\mu}{N} (1+c) \mathbf{J}_B \cdot \mathbf{J}_C, \quad (5)$$

where we introduced $c = \cos(\theta_{AC})$. This Hamiltonian is invariant for a global $SU(2)$ rotation and take as convention the z axis to be flavor axis. We consider two distinct initial configurations diagonal in flavor

(i) $|\Psi_I(0)\rangle = |\uparrow\rangle^{\otimes N_A} \otimes |\uparrow\rangle^{\otimes N_B} \otimes |\downarrow\rangle^{\otimes N_C}$,
 (ii) $|\Psi_{II}(0)\rangle = |\uparrow\rangle^{\otimes N_A} \otimes |\downarrow\rangle^{\otimes N_B} \otimes |\uparrow\rangle^{\otimes N_C}$,
 and $N_A = N_B = N_C = N/3$. In the text we will refer to these initial conditions as setup I and setup II. For both states we have the conserved expectation values

$$\langle \mathbf{J}^2 \rangle_{\Psi_{I,II}} = N^2/36 + N/2 \quad \langle \mathbf{J} \rangle_{\Psi_{I,II}} = (0, 0, N/6). \quad (6)$$

The convention we use throughout is that electron flavor is associated with an up-spin and the heavy lepton flavor ν_x with a down-spin. This rather special choice of initial states was motivated by the fact that a mean-field treatment of their time propagation will result in no flavor evolution and therefore any flavor dynamics is inherently a many-body effect. As mentioned at the beginning of this section, adding a small off-diagonal component leads to an evolving mean-field solution which we will use to characterize the stability of the resulting equation of motion.

III. MEAN-FIELD LINEAR STABILITY ANALYSIS

In the mean-field approximation it is commonly assumed that the correlation between any two neutrinos are negligible: $\langle \mathcal{O}_i \mathcal{O}_j \rangle = \langle \mathcal{O}_i \rangle \langle \mathcal{O}_j \rangle$ where i and j are indices for different neutrinos. Therefore, the time evolution for each neutrino is rewritten as

$$\partial_t \langle \mathbf{J}_i \rangle = \mathbf{H}_{\text{MF}} \times \langle \mathbf{J}_i \rangle = \frac{2\mu}{N} \sum_{j \neq i}^N (1 - c_{ij}) \langle \mathbf{J}_j \rangle \times \langle \mathbf{J}_i \rangle. \quad (7)$$

This mean field approximation can be expected to hold in the limit of large quantum numbers and therefore it is convenient to formulate the evolution equations treating all the neutrinos in a beam at the same time. One can then define a normalized polarization vector for each beam as $\mathcal{P}_\alpha = \sum_{i \in \alpha} \langle \mathbf{J}_i \rangle / (N_\alpha/2)$ and rewrite the equation of motions in terms of \mathcal{P}_α . For our three beam setup we have then

$$\begin{aligned} \partial_t \mathcal{P}_A &= \frac{\mu}{N} [2N_B \mathcal{P}_B + (1-c)N_C \mathcal{P}_C] \times \mathcal{P}_A \\ \partial_t \mathcal{P}_B &= \frac{\mu}{N} [2N_A \mathcal{P}_A + (1+c)N_C \mathcal{P}_C] \times \mathcal{P}_B \\ \partial_t \mathcal{P}_C &= \frac{\mu}{N} [(1-c)N_A \mathcal{P}_A + (1+c)N_B \mathcal{P}_B] \times \mathcal{P}_C. \end{aligned} \quad (8)$$

As we mentioned after the derivation of Eq. (4), the total flavor isospin \mathbf{J} is a conserved quantity. This implies that $N_A \mathcal{P}_A + N_B \mathcal{P}_B + N_C \mathcal{P}_C$ is a constant of motion and therefore only two polarization vectors are dynamical. This is an analogous situation to the one encountered in the two-beam setting leading to bipolar oscillations with the expectation value of the total isospin $\langle \mathbf{J} \rangle$ playing a similar role to the vector \mathbf{B} pointing in the mass basis (see [58]). We will exploit this similarity in Sec. VB when explaining the nature of dynamical phase transitions in the present model (see also [59] for recent work using this similarity in the mean-field approximation).

The instability of the neutrino gas can be diagnosed by analyzing the stability of these differential equations to small perturbations. In the neutrino case, we will then assume that the third component \mathcal{P}_α^z is dominant and linearize the mean-field equations of motion (EOM) in terms of the perturbation away from the flavor axis. Given $N_A = N_B = N_C = N/3$, the linearized EOM for the off-diagonal component $\mathcal{S}_\alpha \equiv \mathcal{P}_\alpha^x - i\mathcal{P}_\alpha^y$ reads

$$\partial_t \begin{pmatrix} \mathcal{S}_A \\ \mathcal{S}_B \\ \mathcal{S}_C \end{pmatrix} = M_{\text{LMF}} \begin{pmatrix} \mathcal{S}_A \\ \mathcal{S}_B \\ \mathcal{S}_C \end{pmatrix} = \frac{\mu}{3} \begin{pmatrix} 2\mathcal{P}_B^z + (1-c)\mathcal{P}_C^z & -2\mathcal{P}_A^z & -(1-c)\mathcal{P}_A^z \\ -2\mathcal{P}_B^z & 2\mathcal{P}_A^z + (1+c)\mathcal{P}_C^z & -(1+c)\mathcal{P}_B^z \\ -(1-c)\mathcal{P}_C^z & -(1+c)\mathcal{P}_C^z & (1-c)\mathcal{P}_A^z + (1+c)\mathcal{P}_B^z \end{pmatrix} \begin{pmatrix} \mathcal{S}_A \\ \mathcal{S}_B \\ \mathcal{S}_C \end{pmatrix}. \quad (9)$$

In the expression above we denoted by M_{LMF} the matrix obtained for the Linearized Mean Field (LMF) equations of motion. The unstable mode of the neutrino gas can be found by parametrizing the time-dependence of the off-diagonal component as $S_\alpha = Q_\alpha e^{-i\Omega t}$ and solving the collective oscillation frequency Ω as the eigenvalues of the matrix M_{LMF} . Any eigenvalues with positive imaginary components imply the existence of modes with exponentially growing amplitudes, which have been associated with the appearance of fast flavor conversion [46,60].

The value of \mathcal{P}_α^z can be either +1 or -1 and depends on the choice of initial conditions. For the state $|\Psi_1\rangle$ from setup I, the eigenvalue equation gives

$$\Omega \left[9 \left(\frac{\Omega}{\mu} \right)^2 - 12 \frac{\Omega}{\mu} + 3 + c^2 \right] = 0. \quad (10)$$

Since the quadratic discriminant $\Delta = 36(1 - c^2)$ is non-negative, there is no flavor instability at the mean-field level. For setup II, we have

$$\Omega \left[9 \left(\frac{\Omega}{\mu} \right)^2 - 6(1 - c) \frac{\Omega}{\mu} + 1 - 4c - c^2 \right] = 0. \quad (11)$$

Since $\Delta = 72c(c + 1)$, when $-1 < c < 0$ two complex conjugate solutions now appear. The instability is associated with the solution with positive imaginary part leading to an off-diagonal component S_α which grows exponentially with time. The unstable solution is

$$\Omega = \frac{(1 - c) + \sqrt{2c(c + 1)}}{3} \mu. \quad (12)$$

When $c = -1/2$, the growth rate reaches the maximum value $\sqrt{2}\mu/6$. The value of Ω for the unstable mode in setup II can be plugged back into the linearized EOM to obtain the following relations of the corresponding eigenvector compared to that of the ν_x beam:

$$\begin{aligned} \frac{|Q_A|^2}{|Q_B|^2} &= \frac{1 + c}{1 - c}, \\ \frac{|Q_C|^2}{|Q_B|^2} &= 1 - \frac{|Q_A|^2}{|Q_B|^2} = \frac{2c}{c - 1}. \end{aligned} \quad (13)$$

The transverse components are associated with flavor transitions in each beam in the linear regime. A larger value for the amplitude $|Q_\alpha|^2$ leads to a higher change of flavor content in the corresponding beam

$$\begin{aligned} |\mathcal{P}_\alpha^z(t) - \mathcal{P}_\alpha^z(0)| &\approx \frac{|S_\alpha(t)|^2}{2} \\ &\approx \frac{|Q_\alpha|^2}{2} \cdot e^{2\text{Im}(\Omega)t}. \end{aligned} \quad (14)$$

When the angular parameter c approaches 0, $|Q_C|^2$ is smaller than $|Q_A|^2$ and the flavor conversion is primarily

associated with beam A rather than C . On the other hand, beam C has more flavor transition when c approaches -1 . While the above relations may not be valid for long timescales, they can describe which ν_e beam is mostly associated with the flavor conversion when the system transits from the linear to the nonlinear regime.

IV. METHODS

In this section we briefly describe the strategy we employ to perform simulations of the three-beam model from Eq. (5) with systems up to $N = 2700$. These system sizes are much larger than what would be possible using the tensor network methods employed in previous works [56,57,61]. Efficient simulations are made possible through an effective use of the angular momentum representation (see [62] for the general method and [55] for an application to a two-beam model).

To give a concrete example, the initial wave function for setup I in this basis is written as

$$|\Psi(0)\rangle = |j_A, m_A\rangle \otimes |j_B, m_B\rangle \otimes |j_C, m_C\rangle, \quad (15)$$

where $j_A = m_A = N_A/2$, $j_B = m_B = N_B/2$, and $j_C = -m_C = N_C/2$. The total flavor isospin of each beam, j_A , j_B , or j_C , is conserved and can be determined from the initial condition. A simplified many-body notation can be introduced as $|\Psi\rangle = |m_A, m_B\rangle$ with only two degrees of freedom, where m_C is determined by m_A and m_B given that the total projection of flavor isospin, $m_A + m_B + m_C$, is conserved. The evolving state is then a linear combination of states with all possible m_A and m_B ,

$$|\Psi(t)\rangle = \sum_{m_A, m_B} a_{m_A, m_B}(t) |m_A, m_B\rangle. \quad (16)$$

We solve the time evolution for the amplitudes of many-body states described above (for more details see appendix B). Once the amplitudes are known, the observables such as polarization and entanglement entropy can be calculated. The projection of flavor isospin for each beam is $\langle J_\alpha^z \rangle = \sum_{m_A, m_B} m_\alpha |a_{m_A, m_B}|^2$. Pair correlations are $\langle J_\alpha^z J_\beta^z \rangle = \sum_{m_A, m_B} m_\alpha m_\beta |a_{m_A, m_B}|^2$. The correlations along the other two directions in flavor space are $\langle J_\alpha^x J_\beta^x \rangle = \langle J_\alpha^y J_\beta^y \rangle = \langle J_\alpha^+ J_\beta^- + J_\alpha^- J_\beta^+ \rangle / 4$, where $J_\alpha^\pm = J_\alpha^x \pm iJ_\alpha^y$. Note that the terms $\langle J_\alpha^+ J_\beta^+ \rangle$ and $\langle J_\alpha^- J_\beta^- \rangle$ are both zero because the net flavor isospin, $m_A + m_B + m_C$, is a conserved quantity for the system, and $J_\alpha^\pm J_\beta^\pm |m_A + m_B + m_C\rangle \propto |m_A + m_B + m_C \pm 2\rangle$, leads to violations of this quantity. Detailed expressions in terms of amplitudes can be found in appendix B.

The Von Neumann entropy is an important measure for the entanglement in a subsystem. For a general multiqubit system divided into two subsystems, \mathcal{A} and \mathcal{B} , the Von Neumann entropy of subsystem \mathcal{A} is defined as

$$S_{\mathcal{A}} = -\text{Tr}[\rho_{\mathcal{A}} \log_2(\rho_{\mathcal{A}})], \quad (17)$$

where $\rho_I = \text{Tr}_B(\rho)$ is the reduced density matrix of subsystem \mathcal{A} . If we take subsystem \mathcal{A} to be beam A , we can write this more explicitly in terms of amplitudes as follows

$$S_A = \sum_{m_A=-N_A/2}^{N_A/2} \left[\left(\sum_{m_B} |a_{m_A, m_B}|^2 \right) \log_2 \left(\sum_{m_B} |a_{m_A, m_B}|^2 \right) \right]. \quad (18)$$

Because setup II can be obtained from setup I by exchanging configurations between beam B and C , all quantities defined can be modified accordingly and not explicitly listed here.

V. RESULTS FOR FLAVOR EVOLUTION

In the following we will first focus on studying the flavor evolution for three beam models in the two setups and show their qualitative differences. In particular, we will compute the survival probability, or persistence, $P_i(t)$ of a representative neutrino in each beam. This can be defined explicitly in terms of the J_i operators as

$$P_{ik}(t) = \frac{1}{2} + \frac{s_{ik}}{N} \langle \Psi_k(t) | J_i^z | \Psi_k(t) \rangle, \quad (19)$$

with $k = 1, 2$ denoting to employed initial state and the constant s_{ik} defined as

$$s_{ik} = \text{sign}[\langle \Psi_k(0) | J_i^z | \Psi_k(0) \rangle], \quad (20)$$

to ensure $P_i(t=0) = 1$ for all neutrinos. For ease of notation, in the following we will denote expectation values at time t as $\langle \cdot \rangle(t)$ dropping the index k indicating the initial condition when no risk of confusion arises.

A. Setup I

The initial wave function for setup I is the product state

$$|\Psi_I(0)\rangle = |\uparrow\rangle^{\otimes N/3} \otimes |\uparrow\rangle^{\otimes N/3} \otimes |\downarrow\rangle^{\otimes N/3}, \quad (21)$$

with equal populations in the three beams. This initial state is symmetric under the exchange $A \leftrightarrow B$ and the Hamiltonian in Eq. (5) remains invariant under this permutation if we also exchange $c \leftrightarrow -c$. In our study of this system we will therefore limit the discussion to positive values of the angular parameter c .

The case with $c = 0$ is special as for this geometry the total spin $J_{AB}^2 = (\mathbf{J}_A + \mathbf{J}_B)^2$ is also conserved and the Hamiltonian takes the simpler form

$$\begin{aligned} H_{ABC}(c=0) &= \frac{4\mu}{N} \mathbf{J}_A \cdot \mathbf{J}_B + \frac{2\mu}{N} (\mathbf{J}_A + \mathbf{J}_B) \cdot \mathbf{J}_C \\ &= N \frac{\mu}{9} + \frac{2\mu}{N} (\mathbf{J}_{AB} \cdot \mathbf{J}_C). \end{aligned} \quad (22)$$

We see then, that up to an overall constant, this case reduces to a two-beam model with unequal population numbers. An exact analytical solution for this scenario was already discussed in Ref. [63] where it was shown that flavor oscillations are present with an amplitude decaying as a polynomial in the population difference $|N_{AB} - N_C| = N/3$. This case recovers the mean field solution qualitatively, which does not show flavor oscillations, in the large system size limit. Our many-body simulations show that this behavior is actually generic for any value of the angular factor $c \neq 1$. The case $c = 1$ is in fact also special as the total spin $J_{AC}^2 = (\mathbf{J}_A + \mathbf{J}_C)^2$ remains conserved and the Hamiltonian becomes

$$H_{ABC}(c=1) = \frac{4\mu}{N} \mathbf{J}_{AC} \cdot \mathbf{J}_B. \quad (23)$$

The crucial difference is however that now the two beams A and C have opposite flavor polarization and their total spin is instead $\langle J_{AC}^2 \rangle = N/3$. A similar situation was also considered in Ref. [63] but the beam had maximal $\langle J_{AC}^2 \rangle$ and $\langle J_{AC}^z \rangle = 0$ initially (i.e., fully polarized in the xy -plane). As the behavior in our case for $c = 1$ is markedly different from the other ones, we first discuss the case $c \neq 1$ and move to $c = 1$ near the end of this section.

We start by looking at the qualitative behavior of the flavor survival probability for $c = 0.5$. In Fig. 2 we show results for the evolution of the survival probability $P_A(t)$ in the first beam as a function of the evolution time and for a variety of system sizes ranging from $N = 12$ to $N = 348$ (indicated with increasingly darker colors for

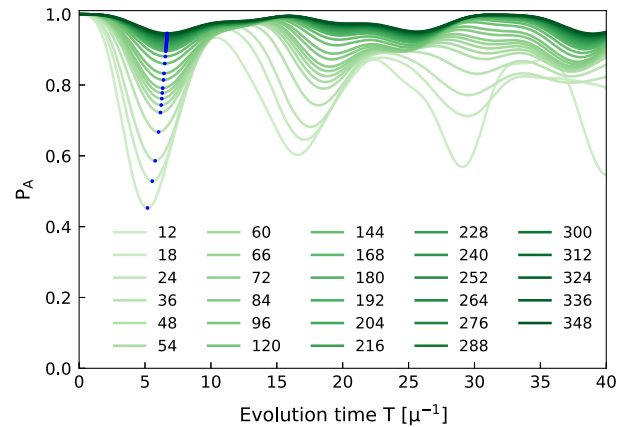


FIG. 2. Time evolution of the survival probability starting in the first beam from the initial state of Setup I and taking $c = 0.5$ for a large selection of system sizes (green solid curves, darker colors indicate progressively larger values of N). With blue dots we also show the location of the first minimum.

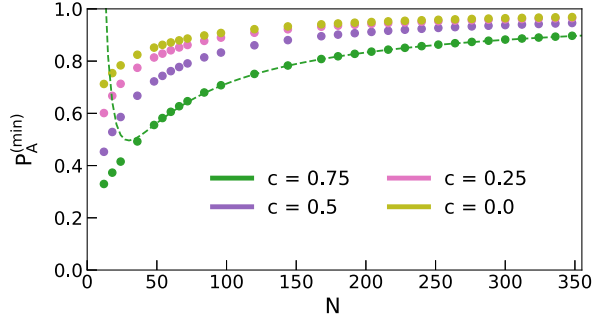


FIG. 3. Evolution with system size N of the value at the first minimum of the survival probability for beam A using the initial wave function $|\Psi_I\rangle$ and various cosine values. The dashed green line corresponds to the best fit for $c = 0.75$ using the parametrization from Eq. (24).

larger systems). The qualitative evolution remains the same for other values of $c \neq 1$ and for different beams.

In order to more easily track the evolution of the amplitude of flavor oscillations in the large N limit, we also show in Fig. 2 the location of the first minimum of the survival probability using blue dots. In the following we will indicate the value reached at the first minimum of the survival probability in beam α as $P_\alpha^{(\min)}$. The results for beam A and different values of the angular distribution parametrized by c are shown in Fig. 3. We find that in all cases the survival probability converges to 1 in the large system size limit. For large but finite $N \gtrsim 50$ the scaling with N is well reproduced by the simple ansatz

$$P_\alpha^{(\min)}(N) \approx 1 - \frac{a}{N} \left(1 - \frac{b}{\sqrt{N}} \right), \quad (24)$$

with $b = \mathcal{O}(1)$ and a increasing with the angular parameter c from $a \approx 13$ at $c = 0$ to $a \approx 45$ at $c = 0.75$. Due to the relatively limited maximum system size considered here, we found the correction term parametrized by b to be important for all angular distributions even though its contribution will vanish in the thermodynamic limit. In Fig. 3 we show the fit performed using Eq. (24) for the case $c = 0.75$ as a green dashed line.

In terms of the expectation value of the spin operators, the scaling from Eq. (24) indicates that in the many-body evolution the expectation value of $\langle J_\alpha^z \rangle$ deviates from its initial value $\pm N_\alpha/2$ only by a constant factor

$$|\langle J_\alpha^z \rangle| \gtrsim \frac{N_\alpha}{2} - a \frac{N_\alpha}{2N} \left(1 - \frac{b}{\sqrt{N}} \right), \quad (25)$$

and the fractional change measured by the z component of the polarization vectors \mathcal{P}_α , defined in Sec. III and used in the mean-field approximation, vanishes for large systems. A similar pattern can also be observed in the other two beams. However, in the second beam we noticed a transient behavior where the first minimum transitions to a stationary

point as the system size increases, and the initial second minimum becomes the first one after $N \approx 100$. Regardless, Eq. (24) remains valid also for this beam for large enough system values (after the transition from first minimum to stationary point).

The timescale to reach the first minimum of the survival probability seems to converge to a constant in the large system size limit agreeing with the expectations from the study in Ref. [63] which were obtained for $c = 0$.

As mentioned above, the case $c = 1$ is peculiar in that the total spin of beams A and C is conserved and kept for all times at a small value $\langle J_{AC}^2 \rangle = N/3$ comparable with the size of quantum fluctuations in the total spin $\langle (J^x)^2 \rangle = \langle (J^y)^2 \rangle = N/4$. Contrary to the previous cases, this allows for quantum fluctuations to drive flavor evolution in a similar way as in the simpler two beam model studied in a previous works (see [56,57,63,64]). Interestingly however, in this case beams A and C are only coupled through their interaction with beam B.

We show the result of our simulation for the survival probability in beam A for this case in Fig. 4. The behavior of beam C is the same while beam B shows little flavor conversion similarly to the results shown in Fig. 2. The top panel shows the evolution of P_A as a function of total time T . This is in marked contrast with the results seen above for $c \neq 1$: the survival probability converges to 0.5 (full mixing) for large times displaying oscillations whose amplitude decays away in the limit of large systems (darker curves in the plot). In order to display more clearly the system size dependence of the timescale to reach the

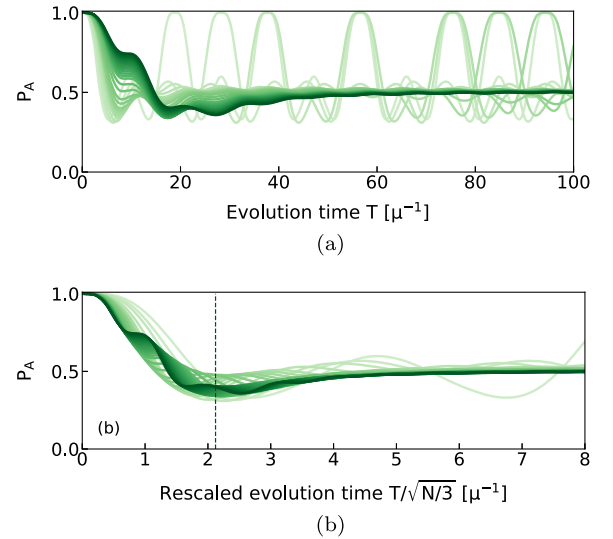


FIG. 4. Time evolution of the survival probability in beam A for the initial state in Setup I, $c = 1$ and the same set of system sizes used for Fig. 2 (darker colors indicate larger values of N). Panel (a) shows directly the time evolution while panel (b) uses a rescaled time variable $T/\sqrt{N}/3$ to highlight the system size dependence. The vertical dashed line in panel (b) indicates the timescale τ_{AC} expected for a two-beam model.

plateau, we also show in the bottom panel of Fig. 4 the same data but as a function of the rescaled time variable $T/\sqrt{N/3}$. These results clearly indicate a decaying timescale $\tau \approx 2\mu^{-1}\sqrt{N/3}$ to reach equilibration at $P_A = 0.5$. Apart from the superimposed oscillations, this is remarkably similar to the behavior shown by a two-beam system, initialized in opposite flavor states. In order to isolate the effective Hamiltonian for the two beams we rewrite

$$H_{ABC}(c=1) = \frac{2\mu}{N}(\mathbf{J}^2 - \mathbf{J}_{AC}^2) - \mu \frac{N+6}{18}, \quad (26)$$

with $\mathbf{J}^2 = \mathbf{J}_{ABC}^2$ the total angular momentum. The two angular momentum operators commute and can then be applied sequentially. The contribution proportional to the total angular momentum is proportional to $H_{ABC}(c=0)$ in Eq. (22) (apart from a constant factor) and, as shown above, does not lead to stable oscillations in the $N \rightarrow \infty$ limit. The large N evolution of the configuration with $c=1$ is then captured by the effective two-beam Hamiltonian

$$H_{AC}^{\text{Beams}} = -\frac{2\mu}{N}J_{AC}^2 = -\frac{4}{3}\frac{\mu}{2N/3}J_{AC}^2. \quad (27)$$

Using the results from Ref. [56], the timescale obtained to reach the minimum of the survival probability would be $\tau_{AC} \approx 3/\sqrt{2\mu^{-1}\sqrt{N/3}}$. This value is reported in panel (b) of Fig. 4 and is seen to match remarkably well the position of the minimum.

Similarly to the standard two-beam case, for this configuration we see that the mean-field prediction of no evolution is recovered as $N \rightarrow \infty$ due to the divergence of the equilibration timescale τ .

In summary the system in Setup I displays the same ‘‘freeze-out’’ behavior described in Ref. [63] for all angular distributions with $c \neq 1$: the polarization vectors in each beam are only able to deviate from their initial values by a vanishing small amount in the large system size limit. The case with $c=1$ is peculiar in that we observe flavor conversion with a system size independent amplitude but a diverging timescale $\tau \propto \mu^{-1}\sqrt{N}$. As we will see in the next section, the presence of instabilities in the system from Setup II, for appropriate values of c , will change this picture qualitatively.

B. Setup II

For setup II the initial product state reads as

$$|\Psi_{II}(0)\rangle = |\uparrow\rangle^{\otimes N/3} \otimes |\downarrow\rangle^{\otimes N/3} \otimes |\uparrow\rangle^{\otimes N/3}. \quad (28)$$

The angular configurations with $c = -1$ is equivalent to the same angle in the previous setup (upon exchanging $B \leftrightarrow C$) and large flavor conversion in beams B and C is seen with a typical timescale $\tau \propto \mu^{-1}\sqrt{N}$. The configuration with $c = 1$ is instead equivalent to $c = 0$ of the previous setup which,

as discussed in the previous section, behaves similarly to the other stable cases in Setup I with a decaying amplitude of flavor oscillations as a function of system size for all beams. In this case the time evolution is however twice as fast due to the presence of an additional factor of 2 in the Hamiltonian [see Eqs. (22) and (23)].

For angular distributions with $c \neq \pm 1$ we can predict the qualitative behavior of the flavor evolution using the same line of reasoning used to obtain the effective Hamiltonian in Eq. (27) above. We first rewrite the Hamiltonian as a sum of two commuting parts to which we have added an unimportant constant, $h = 5\mu(6+N)/6$,

$$\begin{aligned} H_{ABC} + h &= \frac{\mu}{N}\mathbf{J}^2 + \frac{\mu}{N}(\mathbf{J}_{AB}^2 - 2c\mathbf{J}_C \cdot (\mathbf{J}_A - \mathbf{J}_B)) \\ &= \frac{\mu}{N}\mathbf{J}^2 + \frac{\mu}{N}(\mathbf{J}_{AB}^2 - 2c\mathbf{J} \cdot (\mathbf{J}_A - \mathbf{J}_B)) \\ &:= \frac{\mu}{N}\mathbf{J}^2 + H_{ABC}^{\text{dynamic}}, \end{aligned} \quad (29)$$

where in the second line we used the fact that \mathbf{J}_A^2 and \mathbf{J}_B^2 are conserved and take the same value on our initial state. As already commented, the contribution proportional to the total angular momentum does not lead to oscillations in the large N limit and all the flavor dynamics for $c \neq \pm 1$ is driven by the second term denoted as H_{ABC}^{dynamic} . This dominant part of the Hamiltonian is reminiscent of the two-beam Hamiltonian describing bipolar oscillations [55–57]

$$H_{\text{bip}} = \frac{2\mu}{N}\mathbf{J}_{AB}^2 - \delta_\omega \mathbf{B} \cdot (\mathbf{J}_A - \mathbf{J}_B), \quad (30)$$

with the constant vector \mathbf{B} replaced by the total spin of the system \mathbf{J} . In this expression, δ_ω is proportional to the vacuum energy difference in the two beams. This analogy was already pointed out near Eq. (8) above and is consistent with the recent work from Ref. [59] in the mean-field approximation. We can now show that for low energies and large system sizes, the Hamiltonian H_{ABC}^{dynamic} in Eq. (29) has the same properties as H_{bip} and in particular shows the same phase transitions discussed in [57]. Thanks to the all-to-all couplings in the Hamiltonian, the ground state can be approximated accurately with a mean-field state (see [65,57]) so that its energy, can be written as

$$\begin{aligned} E_0(c) &= \frac{2\mu}{N}\langle \mathbf{J}_A \rangle \cdot \langle \mathbf{J}_B \rangle - \frac{2c\mu}{N}\langle \mathbf{J} \rangle \cdot (\langle \mathbf{J}_A \rangle - \langle \mathbf{J}_B \rangle) \\ &= \frac{2\mu}{N}\langle \mathbf{J}_A \rangle \cdot \langle \mathbf{J}_B \rangle - \frac{c\mu}{3}(\langle J_A^z \rangle - \langle J_B^z \rangle), \end{aligned} \quad (31)$$

where we used $\langle \mathbf{J} \rangle = (0, 0, N/6)$. This is exactly the same energy function one obtains with H_{bip} and displays the same quantum phase transitions (see [57]). In particular, for the initial state $|\Psi_{II}(0)\rangle$, we expect to see a dynamical phase transition for $-1 < c \leq 0$ with substantial flavor oscillations and no dynamical flavor evolution for $0 < c < 1$. This is

compatible with the expectations from the mean-field linear stability analysis from Sec. III with the exception of $c = 0$ which was considered stable instead.

The point $c = 0$ is the critical point and dynamics there is expected to happen on timescales $t \approx \sqrt{N}$, as in the marginally stable configurations with $c = \pm 1$ in the previous setup, while for $-1 < c < 0$ flavor evolution should happen on timescales $t \approx \log(N)$. Notably, the frequency of bipolar oscillations generated by the dynamical phase transition in H_{bip} are proportional to $\sqrt{\mu\delta_\omega}$ which is typically much smaller than μ close to the neutrino-sphere. In the multiangle case studied here instead, the coupling constant in front of the one body term in H_{ABC}^{dynamic} is also proportional to μ and this gives rise to oscillations with frequency proportional to μ instead. This suggests that the mechanism behind both bipolar and fast oscillations is the same dynamical phase transition and the difference in timescales is simply given by the difference in coupling constants.

In order to better illustrate the similarity between the dynamical phase transition in the two-beam case leading to bipolar oscillations and the unstable configurations in the present three-beam setup, we now present results for the Loschmidt echo. This is defined as the (squared) overlap between the evolved state $|\Psi(t)\rangle$ and the initial state as follows

$$\mathcal{L}(t) = |\langle \Psi(0) | \Psi(t) \rangle|^2. \quad (32)$$

As discussed more in detail in Refs. [66,67] (see also Ref. [57] for applications in neutrino physics) a dynamical phase transition is signalled by nonanalyticities of the Loschmidt echo as a function of time. For systems with degenerate initial state, as both the two-beam bipolar case for $\delta_\omega = 0$ or the three-beam unstable case for $c = 0$, a suitable generalization of this quantity is obtained as follows (see Refs. [57,68,69])

$$\mathcal{L}_k(t) = |\langle \Phi_k | \Psi(t) \rangle|^2. \quad (33)$$

where $|\Phi_k\rangle$ are the two degenerate states: one is the initial state $|\Phi_0\rangle = |\Psi(0)\rangle$, and the other one is obtained by exchanging the polarization of the A and B beams. In our setup we have then $|\Phi_1\rangle = |\downarrow\rangle^{\otimes N_A} \otimes |\uparrow\rangle^{\otimes N_B} \otimes |\uparrow\rangle^{\otimes N_C}$ for setup II where $|\Psi(0)\rangle = |\Psi_{II}(0)\rangle$. From these definitions of the Loschmidt echo we can also introduce a related quantity, the Loschmidt rate, defined as

$$\lambda(t) = -\frac{1}{N} \log[\mathcal{L}(t)]. \quad (34)$$

Here N is the total number of particles in the system and $\lambda(t)$ an intensive “free energy” [66,70]. The rate $\lambda(t)$ plays here the role of a nonequilibrium equivalent of the thermodynamic free-energy. In cases where the generalization of the Loschmidt echo from Eq. (33) applies, the free

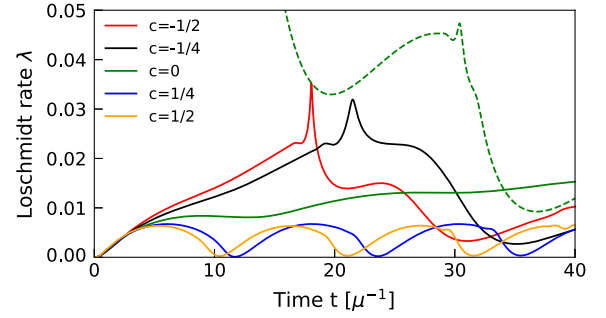


FIG. 5. Loschmidt rate in a system with $N = 348$ neutrino amplitudes initialized in $|\Psi_2(0)\rangle$ of setup II with different values of c : the red and black lines correspond to unstable cases with negative values $c = -1/2$ and $-1/4$ respectively, the blue and orange lines correspond to stable cases with positive values $c = 1/4$ and $1/2$ respectively, and the green line is with $c = 0$ transiting from unstable to stable configuration. Solid lines are for the Loschmidt rate $\lambda(t)$ while dashed line shows the second rate $\lambda_1(t)$ as defined in the text.

energy is given by the minimum of the two rates $\lambda(t) = \min[\lambda_0(t), \lambda_1(t)]$ (see [68]). In these cases, a dynamical phase transition can therefore occur whenever these rates cross for some time t^* , giving rise to a kink in $\lambda(t)$. We present results for these Loschmidt rates at various values of the angular parameter c in Fig. 5. The second Loschmidt rate $\lambda_1(t)$ is shown only for the degenerate case $c = 0$. These results can be directly compared with Fig. 9 of Ref. [57] where the two-beam setup was considered instead. Similarly to that situation, we find that indeed the Loschmidt rates cross for a time $t^* \approx 34\mu^{-1}$ for $c = 0$ while for nonzero values of c the behavior is markedly different between the stable and unstable cases: for stable configurations with $c > 0$ the Loschmidt rate displays periodic oscillations that return to zero while for unstable configurations the Loschmidt rate shows sharp peaks. This is exactly the behavior found in Ref. [57] for the case of slow bipolar modes and suggests that the argument provided above, which links this phenomenon to the fast oscillation case as being produced by the same dynamical phase transition, might be valid. Further work to establish a more robust connection and explore the full dynamical phase diagram of the model is warranted.

As a further confirmation of the stability of configurations with positive values of c , the numerical results we obtain for these configurations show indeed flavor evolution similar to the stable cases observed before, with oscillation amplitudes vanishing as $\approx 1/N$ in the large system size limit.

We can now turn to present the result of our simulation for the survival probability in beam B and $c = -0.5$ in Fig. 6. The time axis has been scaled by the factor $1 + \log N$ to show the system size dependence (darker curves corresponds to larger systems). In Fig. 7 we plot the system size dependence of the time to reach the first minimum in

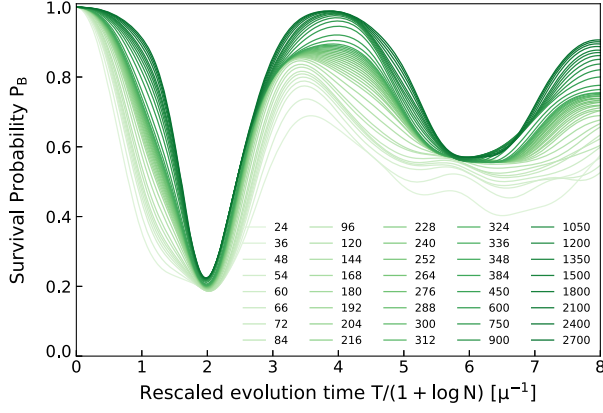


FIG. 6. Time evolution of survival probability in beam B for the initial state in Setup II and $c = -0.5$. The plot uses a rescaled time variable $T/(1 + \log N)$ (darker colors indicate larger values of N) to highlight the system size dependence.

the survival probability in beam B . As expected from the discussion on the presence of a dynamical phase transition in this regime, the time dependence for the unstable configurations with $-1 < c < 0$ is logarithmic $T_B^{\min} \propto \log(N)$. We have observed the same qualitative behavior for all beams and values of c in the unstable region.

The ratios of flavor transitions in each beams during that intermediate stage and their dependence on the angular parameter c are also compared to the mean-field relations in Eq. (13). We pick a time point where the transition probability of beam B , $\Delta P_B \equiv |1 - P_B|$, first reaches a value of $1/2$ ($\sim \mathcal{O}(1)$) to represents an intermediate stage. We calculate the ratio of transition probabilities, $\Delta P_A/\Delta P_B$, at that time, and do the same for all five unstable angular parameters of $c \leq 0$ and two system sizes $N = 384$ and 2700 in Fig. 8. At a larger system size of $N = 2700$, the ratios tend to converge on the prediction from the linear analysis.

However, the long-term evolution of survival probability can deviate from the mean-field result. Within mean-field

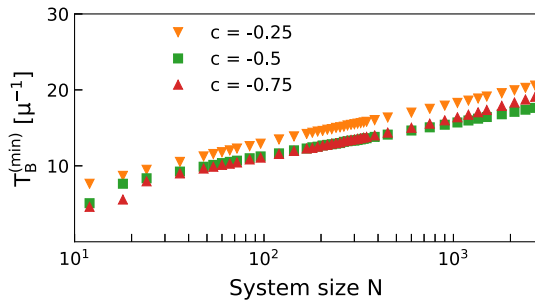


FIG. 7. Time to reach the first minimum in the survival probability in beam B for the initial state in Setup II and different angular distributions as function of system size (on a log scale). The straight lines for $-1 < c < 0$ emphasize the $\log N$ dependence for unstable configurations.

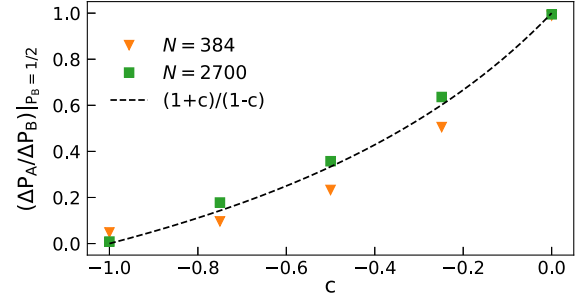


FIG. 8. Setup II: Comparison between the relation of $|Q_A|^2/|Q_B|^2$ in mean-field approximation and the ratio of transition probabilities, $\Delta P_A/\Delta P_B$, in many-body calculations for five unstable parameters of c and two system sizes $N = 384$ and 2700 , respectively.

assumption, this three-beam setup where two beams are antialigned is equivalently an axisymmetric setup and should lead to a bipolar motion with the same minimum survival probabilities in each flavor conversion cycle [48,59], but Fig. 6 shows that the minimal value of survival probabilities in the second cycle (at the rescaled time ≈ 6) is much higher than that in the first one (at the rescaled time ≈ 2) as the system size N goes to 2700 . This deviation is consistent with the behavior of decoherence found in Ref. [62] and will also be reflected by the entanglement and correlations as to be discussed in next section.

VI. ENTANGLEMENT AND CORRELATIONS

In the previous section we studied the dependence of single particle observables like the survival probability on system size. For marginally unstable and unstable configurations we discovered that the many-body result does not converge to the mean field prediction in the large particle number limit. When such a difference appears, one is left to wonder whether the initial mean field wave function evolves with time to a more complicated one. In such a scenario, many-body effects like correlations and entanglement, which would otherwise not be present, tend to develop dynamically [56,57,71,72]. The focus of this section is the study of the pair correlations and entanglement generated during the time evolution.

A. Beam correlations

As we mentioned in the derivation of the mean-field equations in Sec. III, one of the underlying assumptions behind the mean field approximation is the factorization of expectation values $\langle \mathcal{O}_i \mathcal{O}_j \rangle \approx \langle \mathcal{O}_i \rangle \langle \mathcal{O}_j \rangle$ for different neutrinos. Here we explore the violations of this assumptions due to many-body effects by measuring the connected pair correlations along the flavor axis

$$C_{\alpha\beta} = \frac{4}{N_\alpha N_\beta} (\langle J_\alpha^z J_\beta^z \rangle - \langle J_\alpha^z \rangle \langle J_\beta^z \rangle). \quad (35)$$

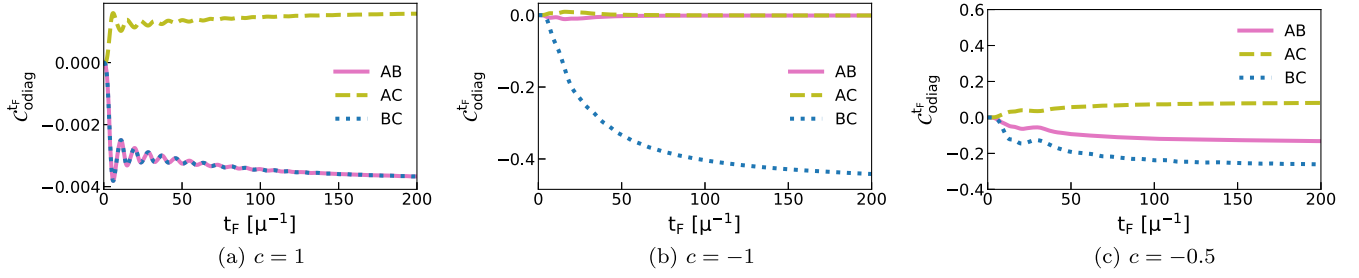


FIG. 9. The time evolution of the three off diagonal pair correlations \mathcal{C}_{AB} , \mathcal{C}_{AC} and \mathcal{C}_{BC} (shown with full, dashed and dotted lines respectively) for the system size $N = 348$. The left panel is a stable system with $c = 1$; the center panel depicts a marginally unstable case with $c = -1.0$, and the right panel shows an unstable case with $c = -0.5$.

We first note that, due to the conservation of the total polarization along the z-axis, the sum for all $\alpha, \beta \in \{A, B, C\}$ becomes

$$\sum_{\alpha, \beta} \mathcal{C}_{\alpha\beta}(t) = \frac{4}{N^2} (\langle (J^z)^2 \rangle - \langle J^z \rangle^2) = 0, \quad (36)$$

where the last equality comes from the initial condition being a product state. This constraint implies that the intrabeam correlations $\mathcal{C}_{A_i A_i}(t)$ are not independent on the correlations $\mathcal{C}_{\alpha\beta}(t)$ between different beams $\alpha \neq \beta$. In particular we have

$$\mathcal{C}_{\text{diag}}(t) = -\mathcal{C}_{\text{oddiag}}(t), \quad (37)$$

where $\mathcal{C}_{\text{diag}}(t)$ and $\mathcal{C}_{\text{oddiag}}(t)$ are the sum of diagonal and off-diagonal pair correlations respectively.

As we have seen in the previous section, for appropriate values of the angular parameter c the three-beam models considered in this work can show flavor evolution in contrast to the mean-field prediction. In these situations we, then, expect correlations to be present as they are responsible for the nontrivial evolution. Since the system in setup II can reproduce all three types of time evolution (stable, marginally unstable, and unstable) we restrict the present discussion to this setup only.

In Fig. 9 we show the time evolution of all three off-diagonal pair correlations for three indicative scenarios and $N = 348$: the left panel shows the case of a stable system with vanishing flavor evolution ($c = 1$), the central panel shows results for a marginally unstable system with flavor evolution at the long timescale $\tau \approx \mu^{-1} \sqrt{N}$ ($c = -1$) and the right panel shows results for an unstable system ($c = -0.5$) with flavor evolution at the short scale $\tau \approx \mu^{-1} \log(N)$. These results show that for stable systems $\mathcal{C}_{\alpha\beta} \approx 0$ at all times, with like flavor beams (A and C) positively correlated and opposite flavor beams anticorrelated. For the marginally unstable system at $c = -1$ the two antiparallel beams B and C whose total spin is conserved are strongly anticorrelated and along times $\mathcal{C}_{BC} \approx -0.5$ while the stable beam A has vanishing correlation with the

other two. Finally, for the unstable case $c = -0.5$, all beams show substantial correlations among each other.

The results shown in Fig. 9 suggest that one can detect instabilities in the neutrino flavor evolution by looking at pair correlations among the beams while the conservation of the total spin also indicates [see Eq. (37)] that correlations must be present inside the beams themselves. These correlations are however influenced by finite size effects and for small system sizes this separation is less pronounced. To show this we present in Fig. 10 the long time average of the total diagonal correlations

$$\mathcal{C}_{\text{diag}}^{t_F} = \frac{1}{t_F} \sum_{\alpha} \int_0^{t_F} dt \mathcal{C}_{\alpha\alpha}(t), \quad (38)$$

as a function of system size N . Due to Eq. (37) we have that $\mathcal{C}_{\text{diag}}^{t_F} = -\mathcal{C}_{\text{oddiag}}^{t_F}$ and the quantities provide a similar measure of correlations. The main panel shows $\mathcal{C}_{\text{diag}}^{t_F}$ in the three cases considered above for $t_F = 400\mu^{-1}$. This value was

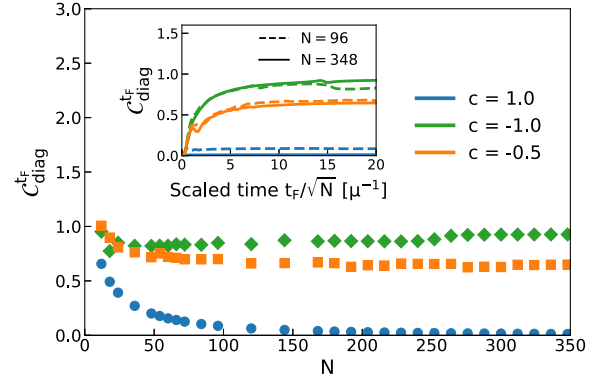


FIG. 10. Evolution with system size N of the long time averaged diagonal pair correlation $\mathcal{C}_{\text{diag}}^{t_F}$ from Eq. (38) for the initial state $|\Psi_{II}(0)\rangle$ and three angular distributions: $c = 1$ (blue circles), $c = -1$ (green diamonds) and $c = -0.5$ (orange squares). The inset shows the dependence on the integration time t_F for the three angular distributions and two system sizes: $N = 96$ (dashed lines) and $N = 348$ (solid lines). The time axis in the inset has been scaled with $1/\sqrt{N}$ to better show the systems size dependence.

chosen to guarantee convergence to the long time average for the largest system considered here, $N = 348$. In general we observe that convergent results can be obtained for all angular distributions choosing $t_F \propto \sqrt{N}$, this is shown in the inset of Fig. 10 where we present the dependence of the time averaged correlations with the size t_F of the time window upon rescaling with \sqrt{N} : the dashed lines correspond to $N = 96$ and the continuous lines to $N = 348$.

B. Entanglement entropy

Another important way to characterize correlations in a many-body system is to estimate the amount of entanglement generated during time evolution. From a practical point of view, entanglement controls the computational cost of classical tensor network methods to simulate the flavor dynamics of a neutrino system. An important example, already used in the study of collective neutrino oscillations in Refs. [56,57], and more recently in [61], are matrix product state (MPS) which can approximate efficiently (i.e., in polynomial cost) quantum states for which the Rényi entropies R_α for any bipartition of the system grow at most logarithmically in the size of the bipartition [73]. We will comment more on the efficiency of a MPS simulation of collective neutrino systems in the conclusions.

Quantum correlations like entanglement are more generally useful tools to analyze the structure of many-body neutrino systems and have been shown to be helpful in detecting the presence of bipolar collective modes in the past [55–57]. These calculations were performed using only two beams and therefore only display slow modes. Here we are interested in extending this connection to fast modes instead, and therefore, might be important near the surface of a proto-neutron star where $\mu \gg \omega$ [43,46]. In [72], the authors found that the largest values of entanglement entropies occur for neutrinos with energies closest to the spectral split energy.

In Fig. 11 we depict, as function of time for $N = 2700$ and the three angular setups from the previous plots, the entanglement entropy S_α [see Eq. (17)] obtained from the reduced density matrix of the *A* beam (full lines) and, for the stable system with $c = 1$, also of the *B* beam (dashed line). For this latter setup, in Figs. 9 and 10 we saw that correlations vanish as the system size increases while entanglement entropy does not. Instead, it rises quickly and then proceeds to oscillate with a relatively small amplitude. For marginally unstable ($c = -1$) and unstable ($c = -0.5$) configurations, the entropy reaches $S^{\max} \approx \log_2(N/3)$. The associated timescales are $t \sim \sqrt{N}$ and $t \sim \log(N)$ respectively, in agreement with our previous observations on the persistence in Sec. V B.

To further confirm the behavior of S^{\max} with N , in Fig. 13 we depict how it scales with system size, with x -axis in log scale, for beam *B*. The stable configuration ($c = 1$) reaches a plateau while the marginally unstable and unstable configurations increase logarithmically. This is

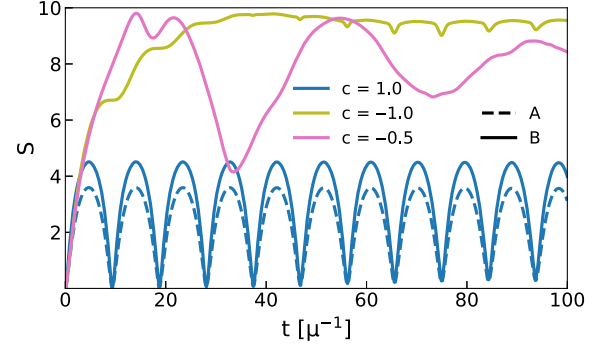


FIG. 11. Entanglement entropy as function of time for system size $N = 2700$. The three angular distributions are $c = 1$ (blue), $c = -1$ (yellow) and $c = -0.5$ (purple). Beam *A* (dashed) is shown only for the stable configuration ($c = 1$) while beam *B* is shown of all three angles.

even more evident by comparing the data from simulations to the line $\log_2(N/3)$ (dashed black line). This logarithmic behavior has also been observed in past MPS based calculations of bipolar oscillations [56,57] as well as more general two-beam models [55].

As the particle number increases, so do the initial expectation values of J_z and \mathbf{J}^2 . Then, for large N we expect to represent the flavor operators $J_\alpha^{x,y,z}$ through canonical bosonic operators, following the Holstein-Primakoff transformation [74] truncated to leading order. If we approximate the state of each beam by a Gaussian, then, the entanglement entropy (Von Neumann entropy) for a beam can be approximated,

$$S_\alpha(t) = \frac{1 + 2\Gamma_\alpha(t)}{\log(2)} \operatorname{arccoth}(1 + 2\Gamma_\alpha(t)) + \frac{1}{2} [\log_2(\Gamma_\alpha(t)) + \log_2(1 + \Gamma_\alpha(t))]. \quad (39)$$

The term Γ_α , related to the covariance matrix of the Gaussian state, can be approximated in two different ways,

$$\begin{aligned} \Gamma_\alpha^{(a)}(t) &= N_\alpha(1 - P_\alpha(t)), \\ \Gamma_\alpha^{(b)}(t) &= \frac{N_\alpha}{4} - \frac{\langle (J_\alpha^z)^2 \rangle}{N_\alpha}, \end{aligned} \quad (40)$$

based on the survival probabilities and correlations, respectively. The detailed analysis can be found in Appendix C. In Fig. 12 we plot the entanglement entropy for beam *B* and $N = 2700$ as function of time, together with the predictions obtained from these two approximations. The panel on the left is a stable system with $c = 1$; the center panel depicts a marginally unstable case with $c = -1.0$, and the right panel shows an unstable case with $c = -0.5$. The survival probability and correlations employed in making this plot were computed with the method described in Sec. IV. For stable configurations, Eq. (39) seems to match the exact result for

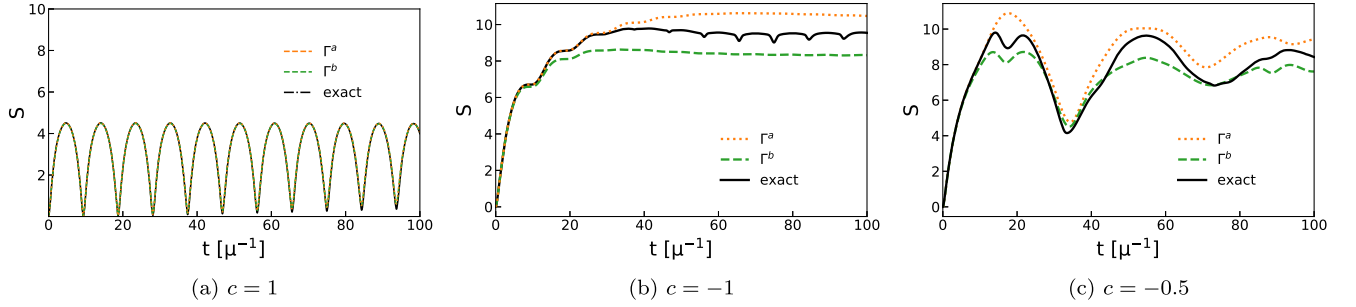


FIG. 12. The time evolution of the entanglement entropy for beam B and the system size $N = 2700$. The left panel is a stable system with $c = 1$; the center panel depicts a marginally unstable case with $c = -1.0$, and the right panel shows an unstable case with $c = -0.5$. The approximation $\Gamma_i^{(a)}(t) = N_i(1 - P_i(t))$ gives a closer result to the exact value than $\Gamma_i^{(b)}(t) = \frac{N_i}{4} - \frac{\langle J_i^z J_i^z \rangle}{N_i}$.

long term dynamics, while for marginally unstable and unstable cases it is a rather good approximation for short time dynamics. The approximation based on the survival probability seems to perform better than the one based on correlations in the marginally unstable case (panel (b)) as it follows the exact evolution for longer times. In the unstable case however, this approximation misses the double peak structure around $t = 20\mu^{-1}$ associated with flavor inversion in the beam (i.e., $P_A < 0.5$), a situation that cannot be described at leading order in the semiclassical expansion (see Appendix C for more details).

These results show that nontrivial evolution of the survival probability is intimately connected to the presence of entanglement and correlations. It would be interesting to extend this approach to more complicated models including a nondiagonal one body Hamiltonian (vacuum frequency) as well as performing the full evolution within the semiclassical approach. In addition, it remains to be seen whether the Holstein-Primakoff approximation is the best choice to represent the system, and, perhaps the truncated Wigner approximation (see [75] and references therein) could also be employed. While their numerical implementation is beyond the scope of this work, if semiclassical treatments are good approximations in the large particle number limit, they may be of practical importance for

simulations relevant for supernovae and neutron star binary mergers.

VII. SUMMARY AND CONCLUSION

In compact objects, core-collapse supernovae and neutron star mergers, neutrinos play a vital role in shaping the dynamics of the system and the conditions for nucleosynthesis in the ejected material. The presence of collective flavor oscillations, primarily due to neutrino-neutrino scattering, could lead to important effects in these aforementioned developments. As these scatterings are dependent only on the angle between particles and couple neutrinos of different energies, flavor evolution is a very complicated many-body problem.

In this work we performed a complete many-body treatment based on the method described in Ref. [62]. We considered a simplified setup of three coplanar beams, parametrized by c —the cosine of the angle between two of the beams, and two neutrino flavors. We focused only the effects due to neutrino scattering and studied the dependence on system size. We selected two initial configurations for the wave function,

- (1) $|\Psi_I(0)\rangle = |\uparrow\rangle^{\otimes N_A} \otimes |\uparrow\rangle^{\otimes N_B} \otimes |\downarrow\rangle^{\otimes N_C}$,
- (2) $|\Psi_{II}(0)\rangle = |\uparrow\rangle^{\otimes N_A} \otimes |\downarrow\rangle^{\otimes N_B} \otimes |\uparrow\rangle^{\otimes N_C}$.

For these setups, the mean field approximation predicts no flavor evolution, and any dynamics is purely a many-body effect. By analyzing the time evolution of the survival probability or persistence for each of the beams, we discovered that for $|c| < 1$ in setup I and $c \geq 0$ in setup II, the many-body results converge to the mean field ones in the large particle number limit. The extremal values of the cosine in setup I and $c = -1$ in setup II denote marginally unstable situations where the survival probability does not converge to 1 as would have been predicted by the mean-field analysis. However, the time to reach its minimum $\sim \mu^{-1}\sqrt{N}$, “freezing” the flavor evolution for large N . The effective Hamiltonian governing these situations is analogous to the two beam system studied in Refs. [56,57] and the results agree with the behavior found there. The system in setup II can instead develop fast collective oscillations

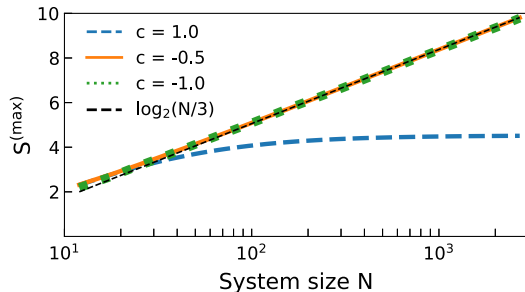


FIG. 13. Maximal value of the entanglement entropy as function of N for beam B, and angles $c = -1$ (dashed blue), $c = -0.5$ (solid orange), and $c = 1$ (dotted green). For comparison, we have also included the $\log_2(N/3)$ (dashed black) functional form to show the system size dependence.

when $-1 < c < 0$ leading to a crossing of the angular distributions. For these cases the persistence does not converge to 1 as N increases and the timescale to reach the first minimum $\sim \mu^{-1} \log(N)$. These unstable configurations can also be derived by rewriting the Hamiltonian to separate the dominant term, which is analogous to bipolar oscillations in the presence of the vacuum term. This establishes a connection between the dynamical phase transition leading to bipolar oscillations and the presence of fast modes. The main difference between the two situations is that now the one body term playing the role of the vacuum frequency there has a coupling proportional to μ . This fact explains in a natural way the distinction between the frequency of oscillations in slow and fast modes. These results are also in agreement with the linear mean field instability analysis we performed in Sec. III. In a follow up work we plan to perform a detailed study of the dynamical phase diagram in this simple multibeam model.

To further confirm the presence of many-body effects, and beyond mean field behavior, we analyzed the entanglement entropy of each beam as well as the time averaged flavor correlations among them. The pair correlations agree qualitatively with the results of the persistence analysis: with increasing system size they vanish for stable configurations but not for marginally unstable or unstable ones. However, the time to reach the plateau scales as $\sim \mu^{-1} \sqrt{N}$ in contrast to the survival probabilities. The entanglement entropies closely resemble the survival probabilities in timescales, and, for unstable configurations reach the maximal values $\approx \log_2(N/3)$.

We have also analyzed the evolution of the entropy using a correspondence between the survival probability and the entanglement entropy in a beam obtained using a semiclassical approximation employing Holstein-Primakoff approximation. This correspondence shows directly that flavor evolution in our system is necessarily accompanied by an increase of the entanglement entropy. The good agreement obtained between this approach and the exact numerical simulations suggests that semiclassical approaches might provide a powerful tool to explore neutrino dynamics in large systems for short time-scales. This will be especially interesting in more complicated situations with a large number of neutrino beams where the angular momentum basis scheme employed here will become computationally too expensive and the entanglement entropy might become too large for tensor network simulations. Finally, simulations using quantum devices [76–78] will likely become important in order to study the long time evolution of these systems.

ACKNOWLEDGMENTS

E. R. acknowledges the NSF N3AS Physics Frontier Center, NSF Grant No. PHY-2020275, and the Heising-Simons Foundation (2017-228). Z. X. was supported by the European Research Council (ERC) under the European

Union’s Horizon 2020 research and innovation programme (ERC Advanced Grant KILONOVA No. 885281). The work of A. R. was supported in part by the U.S. Department of Energy, Office of Science, Office of Nuclear Physics, Inqubator for Quantum Simulation (IQUS) under Award No. DOE (NP) Award No. DE-SC0020970. Calculations were carried out at the Minnesota Supercomputing Institute.

APPENDIX A: THREE BEAM GEOMETRY

We assume the neutrino system is comprised of three beams and the neutrinos in each beam are parallel. This makes for a total of 3 different directions: \mathbf{A} , \mathbf{B} , \mathbf{C} . These vectors form a tetrahedron with volume,

$$V = \frac{ABC}{6} \sqrt{1 + 2c_{AB}c_{AC}c_{BC} - c_{AB}^2 - c_{AC}^2 - c_{BC}^2}.$$

where, c_{AB} is the cosine of the angle between vectors \mathbf{A} and \mathbf{B} . The non-negativity of the volume requires

$$1 + 2c_{AB}c_{AC}c_{BC} - c_{AB}^2 - c_{AC}^2 - c_{BC}^2 \geq 0.$$

For a given volume, two of the three cosines are free parameters. To further simplify our analysis, we assume the three vectors are coplanar and two are antiparallel,

$$c = c_{AC} = -c_{BC}, \quad c_{AB} = -1$$

The corresponding Hamiltonian becomes

$$H_{ABC} = \mu \frac{4}{N} \mathbf{J}_A \cdot \mathbf{J}_B + 2\mu \frac{1-c}{N} \mathbf{J}_A \cdot \mathbf{J}_C + 2\mu \frac{1+c}{N} \mathbf{J}_B \cdot \mathbf{J}_C, \quad (\text{A1})$$

where $N = N_A + N_B + N_C$ is the total number of spins. Note that we used the fact that \mathbf{J}_a^2 is conserved for each one of the beams.

APPENDIX B: THE METHOD IN ANGULAR MOMENTUM REPRESENTATION

The equations of motion for the amplitudes of the many-body state defined in Eq. (16) is

$$\begin{aligned} i\partial_t a_{m_A, m_B} &= T_{m_A, m_B}^{m_A, m_B} a_{m_A, m_B} \\ &+ T_{m_A, m_B}^{m_A+1, m_B} a_{m_A+1, m_B} + T_{m_A, m_B}^{m_A, m_B+1} a_{m_A, m_B+1} \\ &+ T_{m_A, m_B}^{m_A+1, m_B-1} a_{m_A+1, m_B-1} + T_{m_A, m_B}^{m_A-1, m_B+1} a_{m_A-1, m_B+1} \\ &+ T_{m_A, m_B}^{m_A-1, m_B} a_{m_A-1, m_B} + T_{m_A, m_B}^{m_A, m_B-1} a_{m_A, m_B-1}, \end{aligned} \quad (\text{B1})$$

where

$$\begin{aligned}
T_{m_A, m_B}^{m_A, m_B} &= \frac{\mu J_{AC}}{N} [k_C(N_A - k_A) + k_A(N_C - k_C)] \\
&\quad + \frac{\mu J_{BC}}{N} [k_C(N_B - k_B) + k_B(N_C - k_C)] \\
&\quad + \frac{\mu J_{AB}}{N} [k_A k_B + (N_A - k_A)(N_B - k_B)], \\
T_{m_A, m_B}^{m_A+1, m_B} &= T_{m_A+1, m_B}^{m_A, m_B} \\
&= \frac{\mu J_{AC}}{N} \sqrt{k_A k_C (N_A - k_A + 1)(N_C - k_C + 1)}, \\
T_{m_A, m_B}^{m_A, m_B+1} &= T_{m_A, m_B+1}^{m_A, m_B} \\
&= \frac{\mu J_{BC}}{N} \sqrt{k_B k_C (N_B - k_B + 1)(N_C - k_C + 1)}, \\
T_{m_A, m_B}^{m_A+1, m_B+1} &= T_{m_A+1, m_B+1}^{m_A, m_B} \\
&= \frac{\mu J_{AB}}{N} \sqrt{k_A k_B (N_A - k_A + 1)(N_B - k_B + 1)},
\end{aligned} \tag{B2}$$

and k_A , k_B , and k_C are the flipping numbers with $m_A = N_A/2 - k_A$, $m_B = N_B/2 - k_B$, and $m_C = k_C - N_C/2$ respectively. The polarization is related to the projection of flavor isospin

$$P_\alpha = 2\langle J_\alpha^z \rangle / N_\alpha = \sum_{m_A, m_B} \frac{2m_A}{N_A} |a_{m_A, m_B}|^2, \tag{B3}$$

and the pair correlations are

$$\begin{aligned}
\langle J_A^x J_A^x \rangle &= \frac{1}{4} \sum_{m_A, m_B} (N_A + 2k_A N_A - 2k_A^2) |a_{m_A, m_B}|^2, \\
\langle J_A^x J_B^x \rangle &= \frac{1}{2} \sum_{m_A, m_B} \sqrt{k_A k_B (N_A - k_A + 1)(N_B - k_B + 1)} \\
&\quad \times \text{Re}(a_{m_A, m_B+1}^* a_{m_A+1, m_B}), \\
\langle J_A^x J_C^x \rangle &= \frac{1}{2} \sum_{m_A, m_B} \sqrt{k_A k_C (N_A - k_A + 1)(N_C - k_C + 1)} \\
&\quad \times \text{Re}(a_{m_A, m_B}^* a_{m_A+1, m_B}).
\end{aligned} \tag{B4}$$

APPENDIX C: SEMICLASSICAL EXPANSION

In this section we introduce the truncated Holstein-Primakoff transformation, already used in [79,80] for spin systems with long-range interactions, and show how pair correlation in the neutrino beams are directly connected with the entanglement in the system.

As a first step we introduce canonical bosonic operators p_α and q_α for each beams as follows

$$\begin{cases} J_\alpha^x = \sqrt{\frac{N_\alpha}{2}} q_\alpha + \mathcal{O}\left(\frac{1}{\sqrt{N_\alpha}}\right) \\ J_\alpha^y = \sqrt{\frac{N_\alpha}{2}} p_\alpha + \mathcal{O}\left(\frac{1}{\sqrt{N_\alpha}}\right), \\ \pm_i J_\alpha^z = \frac{N_\alpha}{2} - \frac{q_\alpha^2 + p_\alpha^2 - 1}{2} \end{cases} \tag{C1}$$

where the symbol \pm_i denotes a + sign for beams that started in the e flavor (positive z polarization) and a - sign for beams that started in the x flavor (negative z polarization). Note that the commutation relations of the spin operators are preserved only in the asymptotic regime $N_\alpha \gg 1$ for which $J_\alpha^z \approx N_{A\alpha}/2$. This approximation is useful around the limit for which the number of excitations measured by the operator

$$\hat{n}_\alpha = \frac{q_\alpha^2 + p_\alpha^2 - 1}{2} \tag{C2}$$

remains small compared to N_α , a condition that for our system is fulfilled with good accuracy only for stable solutions. We will also approximate the state of each beam as a Gaussian state with covariance matrix

$$G_\alpha = \begin{pmatrix} \langle q_\alpha^2 \rangle & \frac{\langle q_\alpha p_\alpha + p_\alpha q_\alpha \rangle}{2} \\ \frac{\langle q_\alpha p_\alpha + p_\alpha q_\alpha \rangle}{2} & \langle p_\alpha^2 \rangle \end{pmatrix}. \tag{C3}$$

Since we start from a product state we expect this approximation to hold for sufficiently short evolution times. Following the construction in [80], we will use this approximation for the beam wave functions to compute an approximation to the entanglement entropy of each beam. The result reads

$$\begin{aligned} S_\alpha(t) &= \frac{2}{\log(2)} \sqrt{\det G_\alpha(t)} \text{arccoth}(2\sqrt{\det G_\alpha(t)}) \\ &\quad + \frac{1}{2} \log_2 \left(\det G_\alpha(t) - \frac{1}{4} \right), \end{aligned} \tag{C4}$$

where we made explicit the time dependence of the covariance matrix, and thus the entropy. As we can see, the covariance matrix completely characterizes the entanglement properties of a Gaussian state.

In order to calculate the determinant, we first rewrite the diagonal element in terms of spin operators

$$\langle q_\alpha^2 \rangle = \frac{2}{N_\alpha} \langle J_\alpha^x J_\alpha^x \rangle \quad \langle p_\alpha^2 \rangle = \frac{2}{N_\alpha} \langle J_\alpha^y J_\alpha^y \rangle, \tag{C5}$$

due to the $U(1)$ symmetry shared by both the initial state and the Hamiltonian these expectation values remain equal at all times. For the off-diagonal terms instead, we first introduce ladder operators

$$J_\alpha^\pm = J_\alpha^x \pm iJ_\alpha^y = \sqrt{\frac{N_\alpha}{2}} (q_\alpha \pm ip_\alpha), \tag{C6}$$

from which we find

$$\frac{\langle q_\alpha p_\alpha + p_\alpha q_\alpha \rangle}{2} = -\frac{i}{N_\alpha} \langle J_\alpha^+ J_\alpha^+ - J_\alpha^- J_\alpha^- \rangle, \tag{C7}$$

this are also zero for our system due to the conservation of the total spin. We can now proceed in two ways: the first one is to use the definition of $J_{A_\alpha}^z$ in Eq. (C1) to write

$$\begin{aligned}\langle q_\alpha^2 \rangle &= \langle p_\alpha^2 \rangle = \frac{1}{2} + \langle \hat{n}_\alpha \rangle \\ &= \frac{1}{2} + \frac{N_\alpha}{2} \mp_i \langle J_\alpha^z \rangle \\ &= \frac{1}{2} + N_\alpha(1 - P_\alpha(t)),\end{aligned}\quad (\text{C8})$$

where in the last line we avoided the beam-dependent \mp_i sign by using the definition of flavor survival probability for beam i from Eq. (19) of the main text (note that here we have not indicated the initial condition). We can express the covariance matrix as

$$G_\alpha^{(a)} = \left(\frac{1}{2} + N_\alpha(1 - P_\alpha(t)) \right) \begin{pmatrix} 1 & 0 \\ 0 & 1 \end{pmatrix}. \quad (\text{C9})$$

The second one is to use the conservation of the angular momentum J_α^z to write the covariance matrix as

$$\begin{aligned}G_\alpha^{(b)} &= \frac{2}{N_\alpha} \begin{pmatrix} \langle J_\alpha^x J_\alpha^x \rangle & 0 \\ 0 & \langle J_\alpha^y J_\alpha^y \rangle \end{pmatrix} \\ &= \frac{J_\alpha^2 - \langle J_\alpha^z J_\alpha^z \rangle}{N_\alpha} \begin{pmatrix} 1 & 0 \\ 0 & 1 \end{pmatrix} \\ &= \left(\frac{1}{2} + \frac{N_\alpha}{4} - \frac{\langle J_\alpha^z J_\alpha^z \rangle}{N_\alpha} \right) \begin{pmatrix} 1 & 0 \\ 0 & 1 \end{pmatrix},\end{aligned}\quad (\text{C10})$$

where in the last step we have used the initial value $J_\alpha^2 = N_\alpha(N_\alpha + 2)/4$ valid for every beam.

We finally find the following compact expression for the Von Neumann entropy in both approximations as

$$\begin{aligned}S_\alpha^{(a/b)}(t) &= \frac{1 + 2\Gamma_\alpha^{(a/b)}(t)}{\log(2)} \operatorname{arccoth}(1 + 2\Gamma_\alpha^{(a/b)}(t)) \\ &\quad + \frac{1}{2} [\log_2(\Gamma_\alpha^{(a/b)}(t)) + \log_2(1 + \Gamma_\alpha^{(a/b)}(t))].\end{aligned}\quad (\text{C11})$$

In these expression we have introduced the quantity

$$\Gamma_\alpha^{(a)}(t) = N_\alpha(1 - P_\alpha(t)) \quad (\text{C12})$$

for approximation (a) and

$$\Gamma_\alpha^{(b)}(t) = \frac{N_\alpha}{4} - \frac{\langle J_\alpha^z J_\alpha^z \rangle}{N_\alpha}, \quad (\text{C13})$$

for approximation (b). At the beginning of time evolution $\Gamma_\alpha^{(a/b)}(t) = 0$ and so is the entropy. The largest value this can reach in approximation (a) is when the survival probability goes to zero while in approximation (b) when all the angular momentum is in the (X, Y) plane and $\langle J_\alpha^z J_\alpha^z \rangle = 0$. In these limits the entropy is approximately

$$\begin{aligned}S_{\max}^{(a)} &\approx 1 + \log_2(N_\alpha) \\ S_{\max}^{(b)} &\approx 1 + \log_2\left(\frac{N_\alpha}{4}\right).\end{aligned}\quad (\text{C14})$$

Since the (b) approximation depends directly on the approximate definition of the spin operators in the X and Y direction from Eq. (C1), we expect it to break down when $\langle J_\alpha^z \rangle$ deviates significantly from its initial value. On the other hand approximation (a) only relies on this mapping to establish $\langle q_\alpha^2 \rangle = \langle p_\alpha^2 \rangle$ and that the off diagonal elements of G_α are zero but is otherwise exact (within the Gaussian approximation). We then expect approximation (a) to perform better in practice in the limit of large system size.

-
- [1] V. Kosteleck, J. Pantaleone, and S. Samuel, *Phys. Lett. B* **315**, 46 (1993).
[2] K. N. Abazajian, J. F. Beacom, and N. F. Bell, *Phys. Rev. D* **66**, 013008 (2002).
[3] G. Steigman, *Adv. High Energy Phys.* **2012**, 268321 (2012).
[4] B. Follin, L. Knox, M. Millea, and Z. Pan, *Phys. Rev. Lett.* **115**, 091301 (2015).
[5] R. Davis, D. S. Harmer, and K. C. Hoffman, *Phys. Rev. Lett.* **20**, 1205 (1968).
[6] K. Hirata, T. Kajita, M. Koshiba, M. Nakahata, Y. Oyama, N. Sato, A. Suzuki, M. Takita, Y. Totsuka, T. Kifune *et al.*, *Phys. Rev. Lett.* **58**, 1490 (1987).
[7] R. M. Bionta, G. Blewitt, C. B. Bratton, D. Casper, A. Ciocio, R. Claus, B. Cortez, M. Crouch, S. T. Dye, S. Errede *et al.*, *Phys. Rev. Lett.* **58**, 1494 (1987).
[8] E. N. Alekseev, L. N. Alekseeva, V. I. Volchenko, and I. V. Krivosheina, *JETP Lett.* **45**, 589 (1987), http://jetpletters.ru/ps/1245/article_18825.shtml.
[9] Y.-Z. Qian and G. M. Fuller, *Phys. Rev. D* **51**, 1479 (1995).
[10] Y.-Z. Qian and G. M. Fuller, *Phys. Rev. D* **52**, 656 (1995).
[11] A. Mirizzi, I. Tamborra, H.-T. Janka, N. Saviano, K. Scholberg, R. Bollig, L. Hudepohl, and S. Chakraborty, *Riv. Nuovo Cimento* **39**, 1 (2016).
[12] R. D. Hoffman, S. E. Woosley, and Y.-Z. Qian, *Astrophys. J.* **482**, 951 (1997).
[13] H.-T. Janka, *Annu. Rev. Nucl. Part. Sci.* **62**, 407 (2012).
[14] C. Winteler, R. Kppeli, A. Perego, A. Arcones, N. Vassetz, N. Nishimura, M. Liebendrfel, and F.-K. Thielemann, *Astrophys. J.* **750**, L22 (2012).

- [15] S. Wanajo, Y. Sekiguchi, N. Nishimura, K. Kiuchi, K. Kyutoku, and M. Shibata, *Astrophys. J.* **789**, L39 (2014).
- [16] M. J. Savage, R. A. Malaney, and G. M. Fuller, *Astrophys. J.* **368**, 1 (1991).
- [17] J. Pantaleone, *Phys. Rev. D* **46**, 510 (1992).
- [18] J. Pantaleone, *Phys. Lett. B* **287**, 128 (1992).
- [19] S. Pastor and G. Raffelt, *Phys. Rev. Lett.* **89**, 191101 (2002).
- [20] A. B. Balantekin and H. Yüksel, *New J. Phys.* **7**, 51 (2005).
- [21] G. M. Fuller and Y.-Z. Qian, *Phys. Rev. D* **73**, 023004 (2006).
- [22] H. Duan, G. M. Fuller, J. Carlson, and Y.-Z. Qian, *Phys. Rev. Lett.* **97**, 241101 (2006).
- [23] A. Friedland, *Phys. Rev. Lett.* **104**, 191102 (2010).
- [24] M.-R. Wu and I. Tamborra, *Phys. Rev. D* **95**, 103007 (2017).
- [25] G. Fogli, E. Lisi, A. Marrone, and A. Mirizzi, *J. Cosmol. Astropart. Phys.* **12** (2007) 010.
- [26] Y.-Z. Qian, G. M. Fuller, G. J. Mathews, R. W. Mayle, J. R. Wilson, and S. E. Woosley, *Phys. Rev. Lett.* **71**, 1965 (1993).
- [27] Y.-Z. Qian and G. M. Fuller, *Phys. Rev. D* **51**, 1479 (1995).
- [28] H. Duan, G. M. Fuller, J. Carlson, and Y.-Z. Qian, *Phys. Rev. D* **75**, 125005 (2007).
- [29] B. Dasgupta, A. Dighe, A. Mirizzi, and G. G. Raffelt, *Phys. Rev. D* **77**, 113007 (2008).
- [30] J. Gava, J. Kneller, C. Volpe, and G. C. McLaughlin, *Phys. Rev. Lett.* **103**, 071101 (2009).
- [31] H. Duan and J. P. Kneller, *J. Phys. G* **36**, 113201 (2009).
- [32] A. B. Balantekin, *Nucl. Phys.* **A844**, 14C (2010).
- [33] B. Dasgupta, A. Mirizzi, I. Tamborra, and R. Tomas, *Phys. Rev. D* **81**, 093008 (2010).
- [34] H. Duan, G. M. Fuller, and Y.-Z. Qian, *Annu. Rev. Nucl. Part. Sci.* **60**, 569 (2010).
- [35] G. G. Raffelt, *Prog. Part. Nucl. Phys.* **64**, 393 (2010).
- [36] G. G. Raffelt, *Phys. Rev. D* **83**, 105022 (2011).
- [37] H. Duan and A. Friedland, *Phys. Rev. Lett.* **106**, 091101 (2011).
- [38] J. F. Cherry, J. Carlson, A. Friedland, G. M. Fuller, and A. Vlasenko, *Phys. Rev. Lett.* **108**, 261104 (2012).
- [39] J. Pantaleone, *Phys. Rev. D* **46**, 510 (1992).
- [40] H. Duan, G. M. Fuller, and Y.-Z. Qian, *Annu. Rev. Nucl. Part. Sci.* **60**, 569 (2010).
- [41] S. Chakraborty, R. Hansen, I. Izaguirre, and G. Raffelt, *Nucl. Phys.* **B908**, 366 (2016).
- [42] G. G. Raffelt and G. Sigl, *Phys. Rev. D* **75**, 083002 (2007).
- [43] R. F. Sawyer, *Phys. Rev. D* **72**, 045003 (2005).
- [44] R. F. Sawyer, *Phys. Rev. Lett.* **116**, 081101 (2016).
- [45] F. Capozzi, B. Dasgupta, E. Lisi, A. Marrone, and A. Mirizzi, *Phys. Rev. D* **96**, 043016 (2017).
- [46] I. Izaguirre, G. Raffelt, and I. Tamborra, *Phys. Rev. Lett.* **118**, 021101 (2017).
- [47] C. Yi, L. Ma, J. D. Martin, and H. Duan, *Phys. Rev. D* **99**, 063005 (2019).
- [48] L. Johns, H. Nagakura, G. M. Fuller, and A. Burrows, *Phys. Rev. D* **101**, 043009 (2020).
- [49] I. Tamborra and S. Shalgar, *Annu. Rev. Nucl. Part. Sci.* **71**, 165 (2021).
- [50] Z. Xiong and Y.-Z. Qian, *Phys. Lett. B* **820**, 136550 (2021).
- [51] S. Bhattacharyya and B. Dasgupta, *Phys. Rev. D* **102**, 063018 (2020).
- [52] I. Padilla-Gay, S. Shalgar, and I. Tamborra, *J. Cosmol. Astropart. Phys.* **01** (2021) 017.
- [53] S. Bhattacharyya and B. Dasgupta, *Phys. Rev. Lett.* **126**, 061302 (2021).
- [54] M.-R. Wu, M. George, C.-Y. Lin, and Z. Xiong, *Phys. Rev. D* **104**, 103003 (2021).
- [55] J. D. Martin, A. Roggero, H. Duan, J. Carlson, and V. Cirigliano, *Phys. Rev. D* **105**, 083020 (2022).
- [56] A. Roggero, *Phys. Rev. D* **104**, 103016 (2021).
- [57] A. Roggero, *Phys. Rev. D* **104**, 123023 (2021).
- [58] Y. Pehlivan, A. B. Balantekin, T. Kajino, and T. Yoshida, *Phys. Rev. D* **84**, 065008 (2011).
- [59] I. Padilla-Gay, I. Tamborra, and G. G. Raffelt, *Phys. Rev. Lett.* **128**, 121102 (2022).
- [60] A. Banerjee, A. Dighe, and G. Raffelt, *Phys. Rev. D* **84**, 053013 (2011).
- [61] M. J. Cervia, P. Siwach, A. V. Patwardhan, A. B. Balantekin, S. N. Coppersmith, and C. W. Johnson, *Phys. Rev. D* **105**, 123025 (2022).
- [62] Z. Xiong, *Phys. Rev. D* **105**, 103002 (2022).
- [63] A. Friedland, B. H. J. McKellar, and I. Okuniewicz, *Phys. Rev. D* **73**, 093002 (2006).
- [64] A. Friedland and C. Lunardini, *J. High Energy Phys.* **10** (2003) 043.
- [65] F. G. S. L. Brando and A. W. Harrow, *Commun. Math. Phys.* **342**, 47 (2016).
- [66] M. Heyl, A. Polkovnikov, and S. Kehrein, *Phys. Rev. Lett.* **110**, 135704 (2013).
- [67] M. Heyl, *Rep. Prog. Phys.* **81**, 054001 (2018).
- [68] M. Heyl, *Phys. Rev. Lett.* **113**, 205701 (2014).
- [69] B. Žunkovič, M. Heyl, M. Knap, and A. Silva, *Phys. Rev. Lett.* **120**, 130601 (2018).
- [70] A. Gambassi and A. Silva, *Phys. Rev. Lett.* **109**, 250602 (2012).
- [71] E. Rrapaj, *Phys. Rev. C* **101**, 065805 (2020).
- [72] A. V. Patwardhan, M. J. Cervia, and A. B. Balantekin, *Phys. Rev. D* **104**, 123035 (2021).
- [73] N. Schuch, M. M. Wolf, F. Verstraete, and J. I. Cirac, *Phys. Rev. Lett.* **100**, 030504 (2008).
- [74] T. Holstein and H. Primakoff, *Phys. Rev.* **58**, 1098 (1940).
- [75] A. Polkovnikov, *Ann. Phys. (Amsterdam)* **325**, 1790 (2010).
- [76] B. Hall, A. Roggero, A. Baroni, and J. Carlson, *Phys. Rev. D* **104**, 063009 (2021).
- [77] K. Yeter-Aydeniz, S. Bangar, G. Siopsis, and R. C. Pooser, *Quantum Inf. Process.* **21**, 84 (2022).
- [78] M. Illa and M. J. Savage, [arXiv:2202.12340](https://arxiv.org/abs/2202.12340).
- [79] A. Lerose, J. Marino, B. Žunkovič, A. Gambassi, and A. Silva, *Phys. Rev. Lett.* **120**, 130603 (2018).
- [80] A. Lerose and S. Pappalardi, *Phys. Rev. Research* **2**, 012041 (2020).